Supporting Information

Single Cesium Lead Halide Perovskite Nanocrystals at Low Temperature: Fast Single-Photon Emission, Reduced Blinking and Exciton Fine Structure

Gabriele Rainò, [1*] *Georgian Nedelcu,*[2,3] *Loredana Protesescu,*[2,3] *Maryna I. Bodnarchuk,*[2,3] *Maksym V. Kovalenko,*[2,3*] *Rainer F. Mahrt,*[1] *and Thilo Stöferle*[1*]

[1] IBM Research – Zurich, Säumerstrasse 4, 8803 Rüschlikon, Switzerland

[2] Institute of Inorganic Chemistry, Department of Chemistry and Applied Biosciences, ETH Zürich, Vladimir Prelog Weg 1, 8093 Zürich, Switzerland

[3] Laboratory for Thin Films and Photovoltaics, EMPA − Swiss Federal Laboratories for Materials Science and Technology, Überlandstrasse 129, 8600 Dübendorf, Switzerland

Synthesis and Characterization of $CsPb(Cl/Br)_3$ NCs

[see also ref. 19]

Preparation of Cs-oleate. Cs_2CO_3 (0.814 g, Aldrich, 99.9%) was loaded into 100 mL 3-neck flask along with 1-octadecene (ODE, 40 mL, Sigma-Aldrich, 90%) and oleic acid (OA, 2.5 mL, Sigma-Aldrich, 90%), dried for 1 h at 120 ºC, and then heated under N_2 to 150 ºC until all Cs_2CO_3 reacted with OA. Since Cs-oleate precipitates out of ODE at room-temperature, it has to be pre-heated to 100 ºC before injection.

Synthesis of $CsPb(Cl/Br)_3$ NCs. 0.065 mmol $PbCl_2$ (ABCR, 99.999%), 0.122 mmol $PbBr_2$ (ABCR, 98%), 5 mL dried ODE and 1 mL trioctylphosphine (Strem, 97%) were loaded into a 25 mL 3-neck flask and degassed for 10 minutes under vacuum at 120 °C. Afterwards, 1 mL of dried OA and 1 mL of dried oleylamine (Acros Organics, 80-90%) were injected at 120 °C under N_2 flow, causing full solubilization of $PbCl_2$ and $PbBr_2$. The temperature was then immediately raised to 200 °C and 0.4 mL of stock solution of Cs-oleate (prepared as described below) was swiftly injected and 10 seconds later the reaction mixture was cooled down by the water bath. The crude solution was centrifugalized and the supernatant was discarded. Hexane (0.3 mL, Sigma-Aldrich, ≥95%) was added to disperse the NCs and centrifuged again. After centrifugation, the precipitate was discarded and 0.9 mL of toluene (Fischer Scientific, HPLC grade) was added to the supernatant. The NCs were precipitated by adding acetonitrile (0.27 mL, Sigma-Aldrich, ≥99.9%) and by centrifugation. The supernatant was discarded and the precipitate was dispersed in toluene and filtered for further use in optical experiments.

Material characterization. Transmission electron microscopy (TEM) images were recorded using a JEOL JEM-2200FS microscope operated at 200 kV. Temperature-dependent powder diffraction patterns were recorded on a Bruker SMART Platform diffractometer (MoKα-radiation, λ = 0.71073 Å, graphite monochromator) equipped with an Apex-I CCD-detector and a Bruker Kryoflex I cooling system.

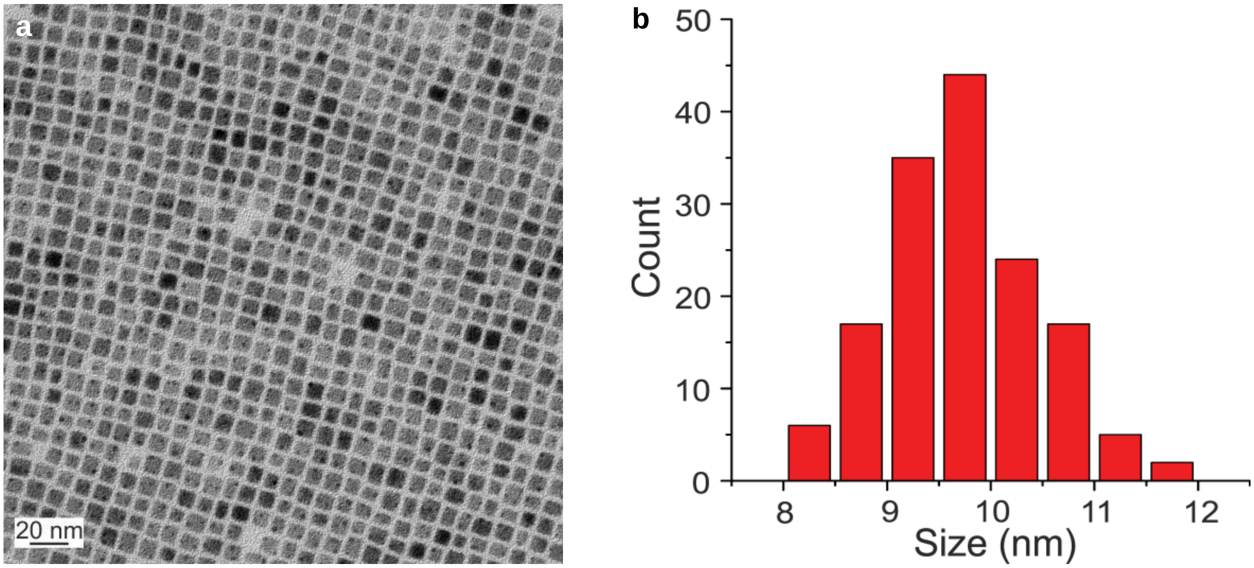

Figure S1. (a) TEM image of a dense monolayer of $CsPb(Cl/Br)_3$ nanocrystals. (b) Histogram of nanocrystal sizes obtained from the TEM image showing a Gaussian distribution peaked near 9.5 nm and size-distribution of *ca.* 10%.

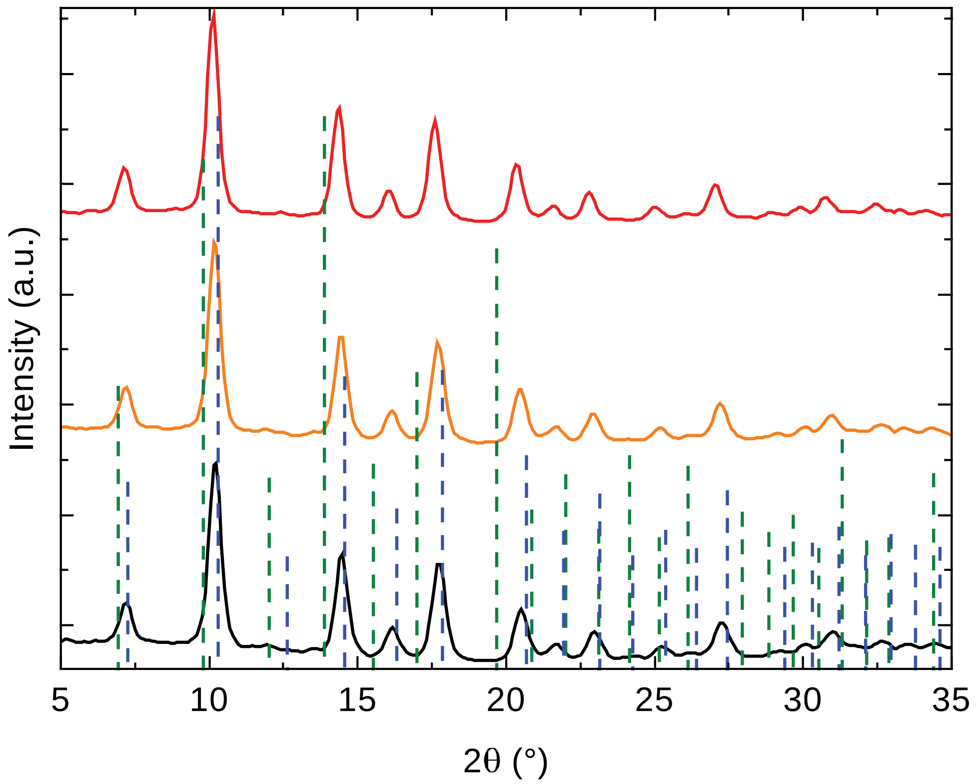

Figure S2. XRD analysis as a function of temperature shows that no phase transitions or phase separation occur when cooling the NCs. Only the usual thermal contraction of the unit cell is observed upon cooling (red 300 K, orange 150 K and black 90 K). The dashed lines mark the room-temperature diffraction peaks of reference samples of pure $CsPbBr_3$ (green) and pure $CsPbCl_3$ (blue) NCs, confirming that $CsPb(Cl/Br)_3$ NCs are homogeneous solid solutions. Notably, all $CsPbX_3$ NCs are formed in the cubic perovskite phase, in which PbX_6 octahedra are three-dimensionally interconnected. On contrary, their bulk counterparts exist exclusively in wider-bandgap one-dimensional orthorhombic phases at ambient conditions.

Intensity Flickering Statistics

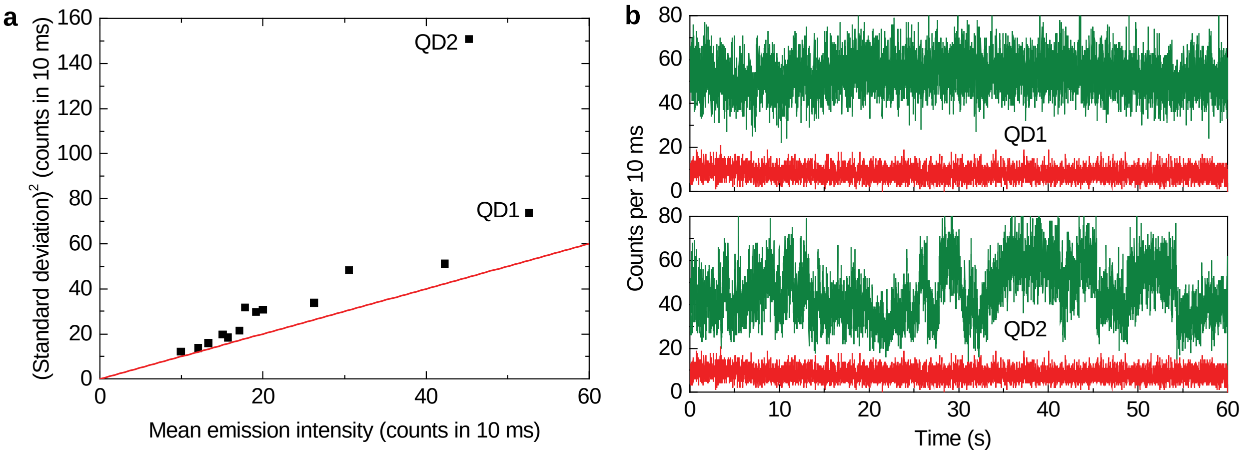

Figure S3. (a) Statistics to quantify the intensity flickering of the QDs. Using a single photon counter, the PL intensity from 13 different QDs are studied at different excitation intensity. The red line shows the expectation for a Poissonian intensity distribution, *i.e.* without any intensity flickering or intermittency. As clearly evidenced by this analysis, the majority of the QDs show a nearly Poissonian intensity fluctuations. (b) Exemplary PL time traces (green) with 10 ms bin time for a particular "stable" (QD1) and a "very flickering" (QD2) quantum dot, as labelled in (a). The red lines show the background that is obtained from near the QDs. No discrete, complete "off" blinking events where the emission drops down to the background intensity are observed as the intensity fluctuations are more gradual on a time scale on the order of a second.

Movie S1 [available online]. The movie shows the PL from an area of 70 x 70 μm on the sample that is excited with (not very homogeneous) wide-field excitation light of λ = 405 nm at intermediate power. This produces more pronounced intensity flickering due to charging effects than at low excitation power, as discussed in the main text. The individual images are captured with 1 s exposure time and are sped up by a factor of 5 for the movie playback. While some QDs are completely stable over the whole measurement time, others exhibit intensity variability on the time scale of several seconds but no permanent photo-bleaching.

Background Subtraction for Time-Resolved PL Measurements

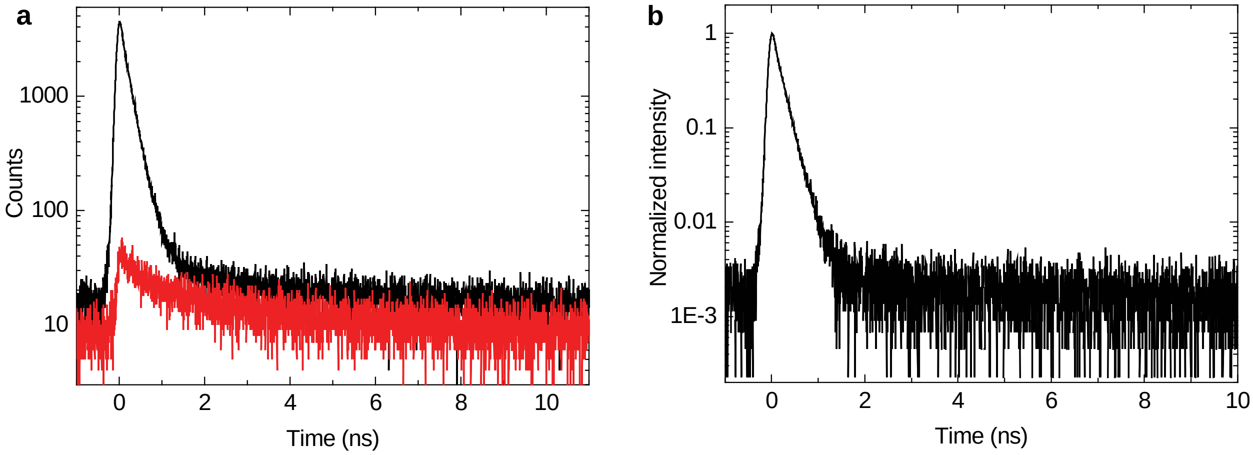

Figure S4. (a) Raw data showing the decay from the QD (black) and from the background (red) near the QD. (b) If the background is subtracted from the QD data, a mono-exponential decay over more than 2 decades is observed. The remaining weak background luminescence (decay time >10 ns) can be quantified to be on the order of 10% of all detected photons, and could have its origin in dark states of the fine structure manifold, (surface) defects or the ligands of the QD.

Photon Anti-bunching Traces

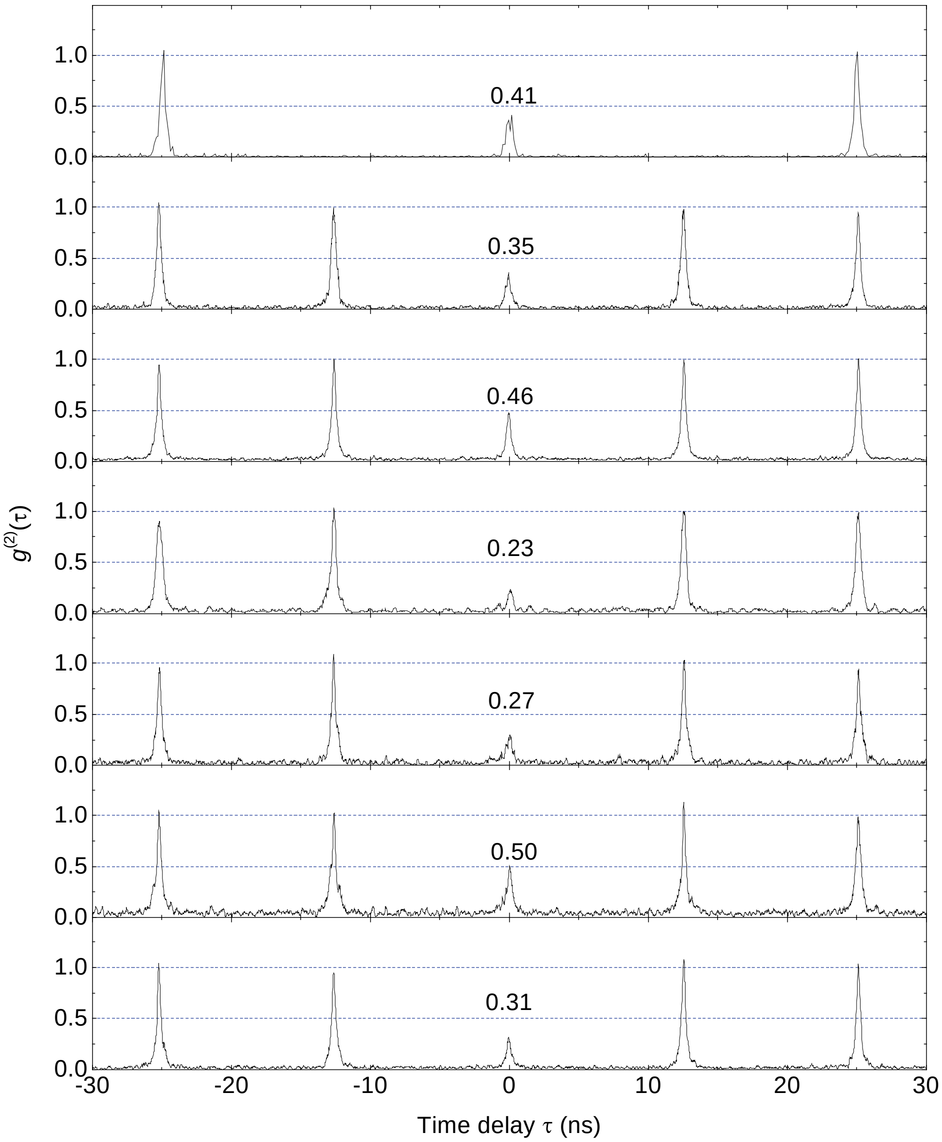

Figure S5. Collection of $g^{(2)}(\tau)$ traces of single QDs obtained from different samples, different synthesis batches and also different excitation sources (most upper trace, pulsed 405 nm diode laser with 40 MHz repetition rate) without any background correction. The corresponding $g^{(2)}(0)$ values are shown in the graphs and range between 0.2 and 0.5 (higher ones are excluded because they might originate not from single QDs) and highlight the independence of the results from several possible systematic effects.

Optical Characterization at Higher Excitation Power

At P_{ex} on the order of few μW the correlations of the emitted photons start to change. This is concomitant with the appearance of multiple emission peaks and an increase in the dynamics in the PL spectrum. These results allow to access the exciton dynamics in the presence of multiple charges within or close to the single QD.

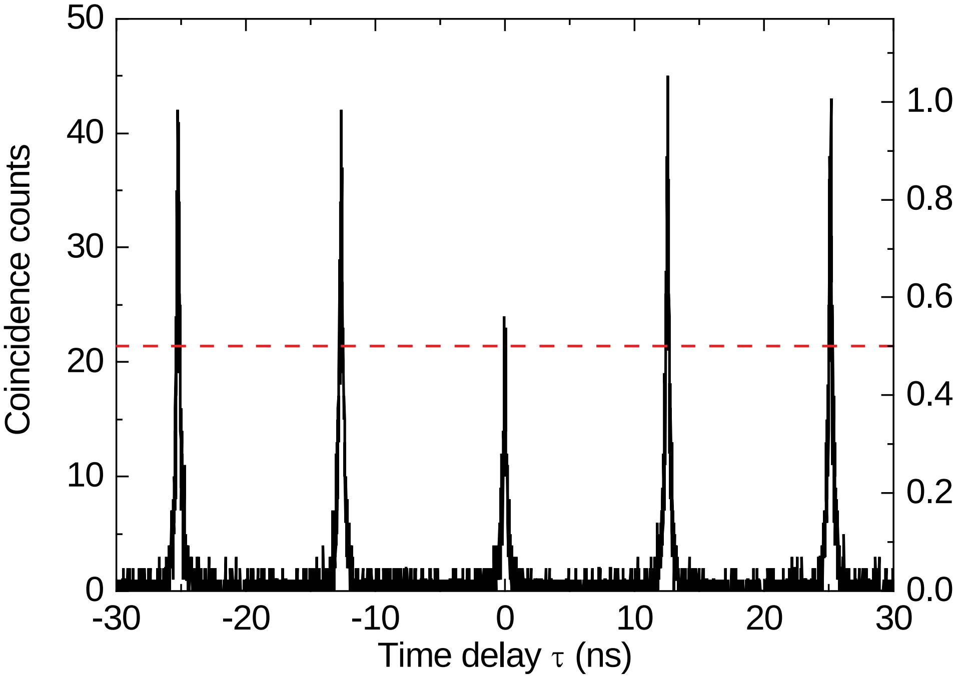

Figure S6. The same QD as in Fig. 3a in the main manuscript is exposed to double the excitation power. Here, the $g^{(2)}(\tau=0)$ changes from 0.3 to 0.55. The integration time is about half the one of Fig. 3a.

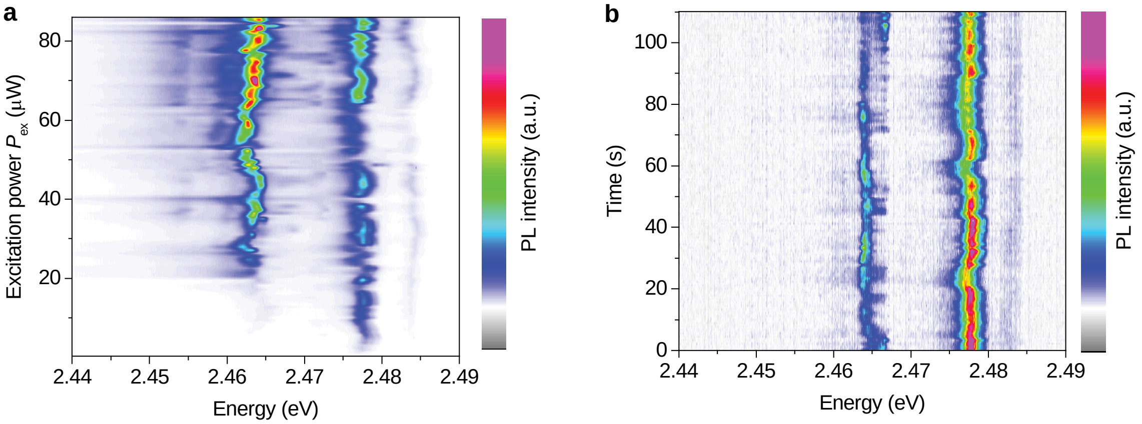

Figure S7. Some QDs show a very rich and dynamic spectrum at high excitation power. (a) Series of spectra as a function of excitation power. Besides the uncharged (2.477 eV) and the charged exciton peaks (2.465 eV), a manifold of peaks appears that is probably related to multi-charge or multi-exciton states. (b) At intermediate excitation power also the spectral diffusion and the intensity flickering is increased. Analyzing the spectra for fixed excitation power, some spectral jumps show correlations between the charged and the uncharged exciton emission, some not. It is expected that screening, dipole moment etc. can be significantly different for both transitions. At certain times, the charged exciton seems to switch between a doublet of two states.